

Soft Granular Particles Sheared at a Controlled Volume:

Flow Curves and Multiple Timescales of Relaxation

J.-C. Tsai ^{a,*}, M.-R. Chou ^{b,a}, P.-C. Huang ^{b,a}, H.-T. Fei ^a, and J.-R. Huang ^{a,#}

a) Institute of Physics, Academia Sinica, Taipei, Taiwan

b) Dept. of Physics, Nat'l Taiwan University

*) jctsai@phys.sinica.edu.tw #) ajrhuang@gate.sinica.edu.tw

We study the responses of fluid-immersed soft hydrogel spheres to both steady shearing and cyclic cessations. The slippery, deformable particles along with the density-matched interstitial fluid are sandwiched between two opposing rough cones, allowing the rheological measurements for volume fractions ranging from 0.73 to 0.27. Steady-state flow curves and shear-to-normal stress ratios reveal nontrivial trends over the decrease of volume fraction. They reflect a solid-to-fluid transition as the system becomes a suspension, with the Reynolds number slightly above unity. In addition, experiments with cyclic shearing and cessations at high volume fractions, accompanied by refractive index-matched internal imaging, establish the connection between stress relaxation and particle rearrangement. Our studies also include the long-time relaxation of the packing as well as that of a single particle. These results demonstrate a multitude of relaxation timescales behind the dynamics of soft particles, and provoke questions on how we extend existing paradigms on the flow of a densely packed system when the softness is actively involved.

{SS3_HGB2019ZotWord_jc20200302d.docx}

Introduction

Soft-matter systems, in many circumstances, exhibit solid-fluid duality. They can be driven to flow steadily and accommodate indefinite amount of shear strain. Meanwhile, the same systems may exhibit a solidity with a resistance to shear, namely, a yield stress. Monitoring the development of yield stress has been a common criterion for the emergence of solidity over the change of controlling parameters including, but not limited to, the volume fraction ϕ or temperature of suspensions^{1,2}. The solidity is sometimes presented in the form of a residual stress upon the cessation of driving, and has been widely studied in glassy systems such as in experiments with synthetic clays or microgels^{3–6}, or in numerical studies including both hard and soft spheres⁷, revealing a wealth of phenomena involving relaxations at different timescales.

Granular materials at high ϕ present interesting examples showing the solid-fluid duality. In the past decades, studies using shear flows have established dimensionless quantities such as inertia number and viscous number that successfully capture behaviors of both dry grains and particle-fluid mixture for a wide range of volume fractions ϕ up to 0.58^{8–11}. As reviewed by Guazzelli and Pouliquen⁹, the current paradigm in theories has assumed Newtonian behaviors, i.e., the stress varying linearly with the shear rate $\dot{\gamma}$ (but with a ϕ -dependent viscosity) at constant volumes, while most supporting experiments and numerical studies are stress-controlled. On the other hand, it is not uncommon that at values of ϕ near the solid-fluid transitions, particle suspensions can exhibit shear-thinning behaviors¹ such that the shear stress is proportional to $\dot{\gamma}^n$ with an index n significantly less than 1 and in many cases close to 0.5^{12–14}. It is also worth noting that all hard-sphere theories would inevitably lose their predictive power on the flow behaviors at volume fractions beyond the “jamming point” -- the current consensus for frictionless particles is the random-close-packing (RCP) $\phi_{RCP} \approx 0.635$, despite some debates had existed with the exact meaning of RCP¹⁵. How we understand the yielding and flow of densely packed soft particles remains a profound challenge. Therefore, further experimental information on the rheological behaviors as well as the shear-induced structural changes across the solid-fluid transition is of vital importance.

In this paper, we start with a survey of steady flows for centimeter-sized hydrogel particles immersed in a density-matched interstitial fluid over a wide range of volume fractions. The results show signs that relaxation of soft contacts, in conjunction with the fluid dynamics at intermediate Reynolds numbers, lead to non-trivial transition of flow curves as the volume fraction changes. Nevertheless, the shear-to-normal stress ratios serves as a good indicator of solid-fluid transition in steady-state experiments. In addition, we present our investigations on the relaxation and the residual stress of the soft packing, using cyclic shearing and cessations accompanied by internal imaging. Our studies demonstrate a wide spectrum of relaxation timescales, for a

jammed packing as well as for a single particle. These results provide clues for further understanding the interplay between the flow imposed at the macroscopic level and the softness of constituent material.

Steady Flows

Shown in Fig.1a, the soft hydrogel particles of diameter $d=1.2\text{cm}$ fill the space between two opposing cones that are roughened by steps comparable to $d/2$. The cylindrical container is made of smooth glass with an inner diameter $2R=23\text{cm}$. The upper cone is set to rotate at a fixed height and with an angular speed Ω driven by a programmable stepping motor with an angular resolution of $2\pi/10^4$. Force sensors attached to the base measure the shear stress and normal stress as functions of time. The gap between the edge of rotating cone and the stationary sidewall is 2mm, and that between the two tips of the cones is 1mm, such that all particles are well contained between two cones. The *volume fraction* is determined as $\phi = N v_1 / (V_{total} - \varepsilon)$ in which $N=O(10^3)$ is the total number of particles. V_{total} represents the total volume between the two cones and v_1 is the average volume of a single particle. The vertical steps (for generating the roughness) and the circumference of the container create certain dead volume that is not accessible, $\varepsilon \sim 0.037 V_{total}$, for our particles with diameter d . Data discussed in this work are based on monodisperse hydrogel particles that are commercially available. Similar products have been characterized independently by previous works^{16,17}. We have confirmed that the response of these hydrogel spheres to normal compression is well described by Hertzian model with the elastic moduli $E \sim 30\text{kPa}$. In addition, we have verified that the friction coefficients of the particle-particle and particle-sidewall contacts are well below 0.01. For all experiments discussed in this paper, particles are fully immersed in the aqueous solution of 1.7% PVP-360 (polyvinylpyrrolidone) to achieve density match that prevents sedimentation. The viscosity of the PVP-360 solution is $\eta = 8\text{mPa}\cdot\text{s}$. Simultaneously, we take internal images of particles at the mid-height of the packing, with details to be described in a later session.

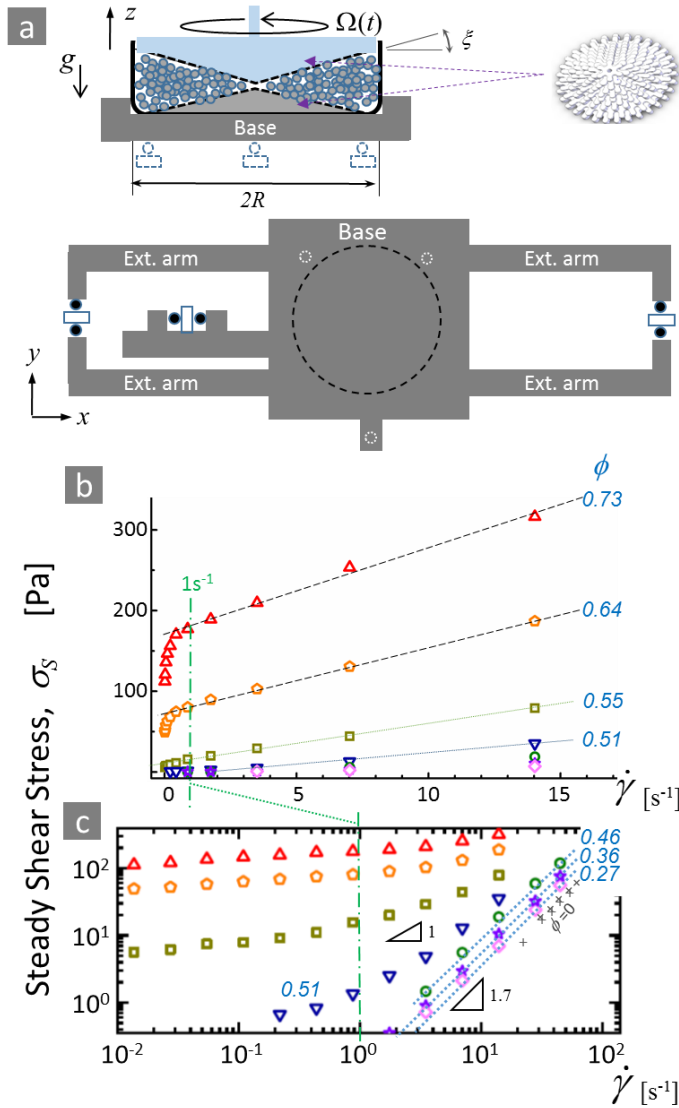


Fig. 1 (a) Vertical cross-section of the setup, definition of symbols, and an angled view of the cone structures. Lower part shows a top view of the base and extended arms. The base is constrained by six force sensors (empty rectangles) that are fixed on a rigid supporting system (not shown). **(b-c)** Time-averaged shear stress σ_s as functions of the shear rate $\dot{\gamma}$, at different values of ϕ . Data are time-averaged for a strain accumulation over 100 for each point, and are plotted in linear and logarithmic scales, respectively. In the logarithmic plots, slopes of 1 and 1.7 are shown as guides to the eyes. Data with pure fluids ($\phi=0$) are displayed with crosses for experiments using the standard PVP solution but with plus signs for experiments using water --- these data points overlap with each other within our measurement uncertainty.

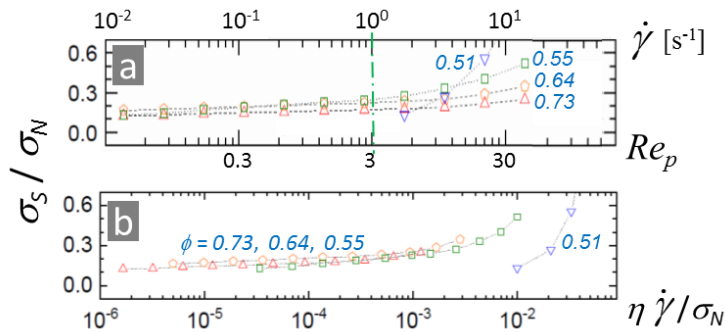


Fig. 2 Shear-to-normal stress ratios, plotted against the particle Reynolds number (a) and the viscous number (b), respectively, for steady-state experiments at four representative volume fractions. As a reference, the shear rate 1s^{-1} is indicated in (a) by the same vertical dash-dot line as that in Fig.1(b-c)

Flow curves

Figure 1b shows the measured steady-state shear stress, $\sigma_S \equiv 3 \text{ torque} / 2 \pi R^3$, plotted against the effective shear rate $\dot{\gamma} \equiv \Omega / (2 \tan \xi) = 13.7 \cdot \Omega / 2\pi$ for several values of ϕ . For $\phi = 0.64$ and 0.73 , the high- $\dot{\gamma}$ data ($\dot{\gamma} > 1 \text{ s}^{-1}$) are well fitted by the Bingham model, i.e., σ_S is linearly dependent on $\dot{\gamma}$ with a nonzero offset, as shown by the dashed lines. However, σ_S at low shear rates deviates significantly from the linear extrapolation of the high-shear data; measured values go significantly lower than the Bingham offset as the shear rate further decreases. Such deviation occurs at the shear rate around 1 s^{-1} . This suggests that, when particle contacts are maintained for 1s or longer, there are additional factors other than just the elasto-hydrodynamic that reduces the shear stress--- We will revisit this subject and show a multitude of timescales for these soft particles to relax, in subsequent sessions.

Many prior experiments^{1,12} have adopted Herschel-Bulkley model (HB, $\sigma_S = \sigma_Y + K \dot{\gamma}^n$) and successfully determined a well-defined jamming density by analyzing the transition of σ_Y . However, the HB-fit with our data presents certain difficulties. At a high volume fractions, the fitting results appear sensitive to the range of data included*. Meanwhile, for ϕ as low as 0.51 , the convexity of the curve in Fig.1c seems gives a non-zero value of σ_Y . However, this outcome is unphysical as our further experiments have shown that this volume fraction is already below the limit for exhibiting solidity --- the system has become a suspension. One reason that HB model is unsuitable for our analyses is that the Reynolds number of our suspension is in the intermediate range: Once we have a suspension with $\sigma_Y = 0$, it would be impossible for our experiment to exhibit one single logarithmic slope ($\sigma_S \sim \dot{\gamma}^n$) because our window of observation covers a crossover of the Reynolds number, which we will explain subsequently.

Stress ratios

We find that the stress ratio σ_S / σ_N , where $\sigma_N \equiv F_z / \pi R^2$, turns out to be a good indicator for characterizing the solid-fluid transition. In Fig.2, we plot σ_S / σ_N against two dimensionless variables: (a) the *particle Reynolds number* $Re_p \equiv \rho \left(\frac{d}{2}\right)^2 \dot{\gamma} / \eta$, which quantifies the relative importance of the *inertial force* in comparison with the *viscous stress* in a conventional suspension; and (b) the *viscous number* $J \equiv \eta \dot{\gamma} / \sigma_N$ which weights the viscous stress over the *total pressure*, as is commonly used in the studies of dense granular suspensions⁹.

* For the case $\phi = 0.71$, σ_Y goes from a high value of 160Pa (with $n=1$, for data above 1 s^{-1} only) to as low as 50-100Pa (with $n < 1$, by including more data at slower shear rates.)

For $\phi = 0.73, 0.64$, and 0.55 , Fig. 2a reveals that the stress ratio σ_S/σ_N is roughly rate-independent (≈ 0.14) in the small- Re_p regime. This observation largely agrees with a previous prediction from simulations of nearly rigid frictionless particles in the quasi-static regime¹⁸, but ours has extended to the cases that substantial deformation of particles is expected with $\phi = 0.73 > \phi_{RCP}$. The curve of σ_S/σ_N changes dramatically as ϕ decreases by just 0.04 (from 0.55 to 0.51), in comparison to the relatively mild change from 0.73 to 0.55. The above observations can be understood as the competition between the solidity of the internal structure and the influence of fluid. At high ϕ , all particles are in tight contact with multiple neighbors and behaves like a solid: the macroscopic shear stress originates mainly from the anisotropy of the contact which converts the compression to a shear stress. The contribution from the viscous fluid plays little role in comparison to the force of direct contact, and so does its potential rate dependence.

However, as the volume fraction decreases, particles would eventually lose direct contact and the packing becomes a suspension. In our experiments, the particles and fluids are density-matched at $\rho = 1.2$ g/c.c. and both the particle diameter d and the interstitial fluid viscosity η are fixed. The Reynolds number Re_p can be treated simply as a dimensionless shear rate. Readers could cross-reference Fig. 1c and Fig.2a and find that our data for $\phi = 0.73, 0.64$, and 0.55 span from the small- Re_p regime ($Re_p < 1$, where the effect of inertia is unimportant) to the large- Re_p regime ($Re_p > 1$, where the contribution of inertia can be substantial even though the contacts still dominate the dynamics). As the system becomes a suspension for $\phi = 0.51$, even though the shear stress σ_S at small- Re_p regime is mostly below our detection limit, our detectable σ_S starts with the shear rate with a Reynolds number $Re_p \sim 1$ that gradually increases. The result is the σ_S at this volume fraction does not show a constant logarithmic slope and exhibits a convexity on Fig.1c. But for $\phi < 0.51$, all data points are obtained in the regime with $Re_p \gg 1$, and they show a simple, constant logarithmic slope with $\sigma_S \sim \dot{\gamma}^{1.7}$. In fact, based on our previous work in a similar geometry¹⁹, we deduce that these dilute flows are in the regime where fluid inertia can induce secondary vortex. The dominance of inertia also explains why the shear stress appears insensitive to the viscosity at the limit of $\phi = 0$ in this experiment --- see the good overlap of data points for pure water ($\eta \sim 1$ mPa · s) and those for our standard PVP-360 solution ($\eta \sim 8$ mPa · s).

We also find that plotting the stress ratio σ_S/σ_N against the viscous number $J \equiv \eta \dot{\gamma} / \sigma_N$ provides a clearer indication of the solid-fluid transition --- see Fig.2b. For a solid-like packing at high ϕ , one would anticipate that σ_N would be dominated by *particle-particle contacts*. The good collapse of data point for $\phi = 0.73, 0.64$, and 0.55 seems to extend the previous finding that the stress ratio can indeed be well characterized by a single dimensionless number J for multiple volume fractions in granular suspensions⁹. Nevertheless, our measurements are made for much denser packing of particles than in previous studies. Reduction of volume fraction to $\phi = 0.51$ creates a clear separation of the curve from those at higher volume fractions, providing an unambiguous sign of the solid-fluid transition.

Response to Cyclic Shear Cessations

To supplement the studies of steady states, we perform experiments with cyclic shear cessations (CSC). Our CSC is defined by two characteristic times, Δ_{On} and Δ_{Off} , plus a constant rate $\dot{\gamma}^{(P)}$ imposed in alternating directions, as shown in Fig.3a. By precision optical measurements, we have verified that the rotating boundary stops abruptly within 10ms in either direction. Fig.3b shows the typical response in the effective stress in analogy to that defined in steady-state experiments. The nearly periodic response provides two pairs of characteristic values. (1) In the mobile period, the system undergoes a short transient (in comparison to Δ_{On}) and reach two plateaus ($|\sigma_S^{(P)}|$, $\sigma_N^{(P)}$). (2) The stress does not just vanish after the abrupt stops of the driving boundary. Rather, two residues ($|\sigma_S^{(R)}|$, $\sigma_N^{(R)}$) remain as a “memory” for the previous direction²⁰: These non-zero residues show that our tight packing is an interesting contrast to an over-damped suspension (--- see Fig.1 of the cited reference), in which sudden cessations of shearing leave no residues but the memory shows up upon the starting of the next mobile period.

In Fig.3(c-d) we compare results from experiments at five different volume fractions. Note that at $\phi=0.55$, only $|\sigma_S^{(P)}|$, $\sigma_N^{(P)}$ and $\sigma_N^{(R)}$ are displayed. The $|\sigma_S^{(R)}|$ is undefined because detected values scattered severely and are below the noise level. This fact reinforces that $\phi=0.55$ is indeed at a marginal state for the solid-fluid transition, as we will revisit this case with evidence from imaging in a subsequent session. It is worth noting that $\phi=0.55$ coincides with the Random Loose Packing density (RLP) as pointed out by a previous work²¹.

Note that the stress after the sudden cessation of boundary movement has a measurable, long-lasting relaxation, which will be examined in detail in the next subsection. For consistency, the values of residual stress in Fig.3d are determined at $\Delta_{\text{Off}}=120\text{s}$, for all volume fractions. Both the plateaus and residues in Fig.3c-d are reproducible, with the stochastic variation smaller than the size of the symbols.

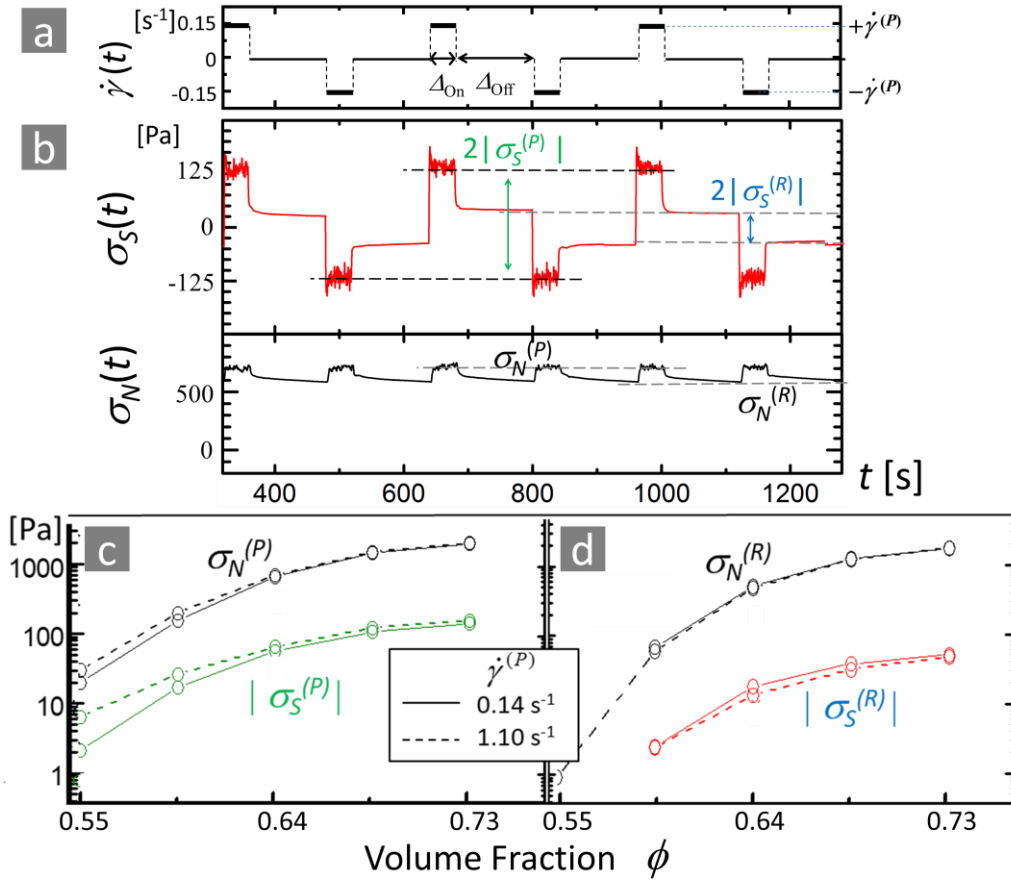


Fig. 3 Stress measurements with cyclic shear cessations ---- **(a)** Protocol of CSC as demonstrated by the time-dependent shear rate $\dot{\gamma}(t)$; **(b)** The time-dependent shear and normal stress in response to the CSC, as well as illustrations of the plateau values, $|\sigma_s^{(P)}|$ and $\sigma_N^{(P)}$, and stress residues, $|\sigma_s^{(R)}|$ and $\sigma_N^{(R)}$. Sample signals are shown for the case of $\phi = 0.73$, with a smoothing by 0.1s to suppress the random noise. **(c-d)** Plateau values and residues as functions of ϕ , in experiments with two different values of $\dot{\gamma}^{(P)}$ and $\Delta_{\text{Off}} = 120 \text{ s}$, $\dot{\gamma} \Delta_{\text{On}} = 5.5$. In both (c) and (d), statistical variations among different cycles are all within the size of the symbols.

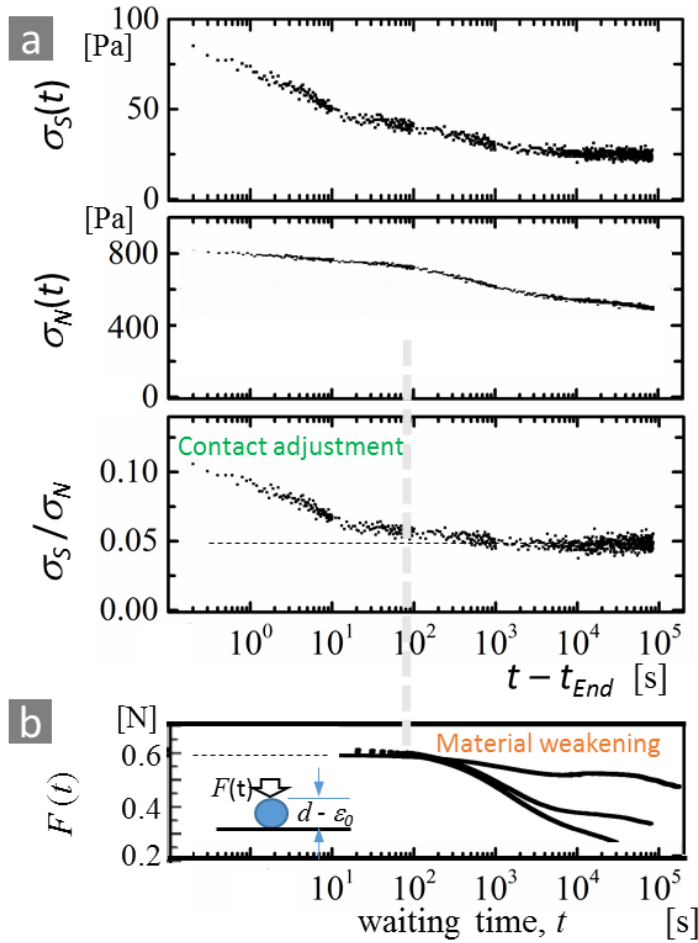


Fig. 4 (a) Time evolution of stress residues following a long stall, in terms of the shear stress, normal stress, and their ratio. The packing has a volume fraction 0.73. The offset t_{End} marks the last stop of a CSC protocol of 25 cycles in which $\dot{\gamma}^{(p)}=0.137s^{-1}$. **(b)** Time evolution of the normal force $F(t)$ measured for a single particle at a fixed uni-axial compression ε_0 . The particle is immersed in the same fluid as that in (a), stress-free for $t < 0$, and a compression is imposed to create an initial condition $F(0+)=0.6N$ that stays constant at the timescale of 10-100s. The graph shows the data from three randomly chosen particles.

Relaxation of the soft packing

To understand the relaxation of packing at a high-volume-fraction state, we perform an experiment with a long stall added to the end of our typical CSC protocol (of 25 cycles). Figure 4a presents the evolution of the shear and normal stress, respectively, as well as the stress ratio as functions of time. Note the logarithmic scale in time. The shear stress decays faster in the first three decades than in the last three. On the other hand, the decay of normal stress has a different feature and appears to become steeper beyond 10^2 s. Both σ_S and σ_N have decreased by more than 25 percent between 10^2 s and 10^5 s.

The shear-to-normal stress ratio, σ_S/σ_N , shows a rapid initial decay in the first 10^2 s, but is stabilized beyond 10^3 s. The rapid decay implies a reduction of structural anisotropy due to particle rearrangements, which we will demonstrate with internal imaging subsequently. The substantial decay of total stress between 10^2 s and 10^5 s but with a fixed stress ratio, on the other hand, suggests the weakening of the hydrogel particles themselves with an isotropic decay of mean stress over time. In what follows, we test our conjecture on the weakening of hydrogel with an experiment at the single-particle level.

Weakening of a single particle

To probe whether the strength of individual grains gradually weakens, we monitor the response of a single hydrogel particle to a fixed compressional strain over long time. Shown as in Fig.4b, the particle is compressed to $d - \varepsilon_0$ and stay fixed. The initial condition $F(0+)=0.6$ N is about ten times of $d^2\sigma_N$ to mimic the situation of those load-bearing particles inside a high-volume-fraction packing. Multiple long-time experiments confirm that (1) the hydrogel maintains its strength up to about 100s, and that (2) hydrogel particles do weaken significantly at larger timescales. The fact (2) confirms our conjecture that material weakening is involved in the long-time decay of stress. In addition, the fact (1) in combination of the stabilized stress ratio at 10^2 s justifies our choice of $\Delta_{\text{Off}}=120$ s for evaluating the residual stress in Fig.3.

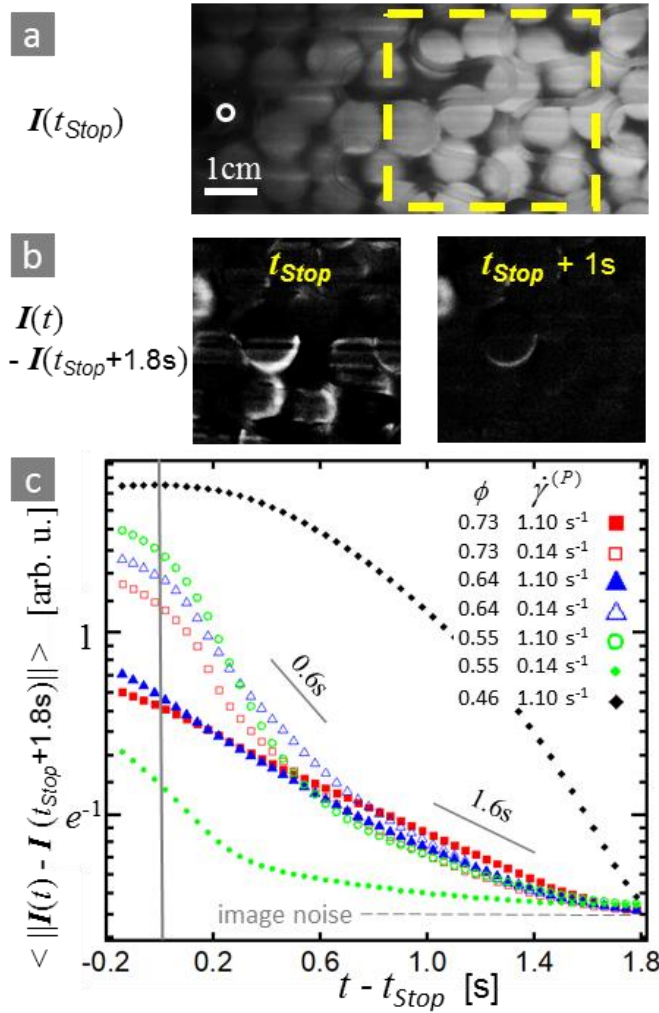


Fig.5 Rearrangement of particles along the mid-height. **(a)** Snapshot of an original image at a volume fraction 0.73. The empty circle on the left indicates the center of the container. **(b)** Two images subtracted by the same reference frame at $t_{stop} + 1.8s$, for the region bounded by the dashed square in (a). Timestamps are shown in the image. **(c)** Summation of the pixel intensity for the subtracted images, plotted against the time elapsed, $t - t_{stop}$, and phase-averaged over multiple cycles. Data include results from different combinations of ϕ and $\dot{\gamma}^{(P)}$. Two short lines show exponential decays at time constant $\tau_1=0.6s$ and $\tau_2=1.6s$, respectively, as guides to the eyes.

Short-time rearrangements

Fluorescent internal imaging allows us to monitor the rearrangement of particles during relaxations^{22,23}. Here, we stain these hydrogel particles with Nyle Blue, and illuminate them at the mid-height by a 1mm-thick laser sheet at a wavelength 635nm ---- see Fig.5a showing a close-up of the bandpassed image (at $656 \pm 10\text{nm}$). Notably, transient rearrangements have been predicted in numerical studies with parameters for microgels³. Our experiments present a direct visual demonstrations of such effects but in the context of a centimeter-sized granular packing.

We record images over multiple cyclic shear cessations. The observation time window is chosen to be $[t_{\text{Stop}} - 0.2\text{s}, t_{\text{Stop}} + 1.8\text{s}]$, where t_{Stop} represents the moment that the driving stops abruptly. The choice is based on the fact that, for a high-volume-fraction packing, movements beyond a few seconds are too small to be distinguished from pixel noises. Fig.5b displays the subtraction by the last frame as a reference, to illustrate the rapid decay of structural rearrangement. In Fig.5c, we quantify the time evolution by a summation over pixel intensities of the subtracted images, with the value averaged over 25 cycles. Experiments at different shear rate $\dot{\gamma}^{(P)}$ and volume fraction ϕ share exactly the same illumination, and are compared as follows.

At $\phi = 0.73$ and 0.64 , particles are tightly packed and one would anticipate substantial storage of elastic energies. At the slow shear rate $\dot{\gamma}^{(P)} = 0.14\text{s}^{-1}$, one could interpret the flow with a quasi-static picture: The agitation is low, so that the difference between the mobile period (Δ_{On} , before t_{Stop}) and “static” period (Δ_{Off} , after t_{Stop}) is insignificant. The curves look like a smooth continuation across t_{Stop} . On the other hand, the higher shear rate of $\dot{\gamma}^{(P)} = 1.10\text{s}^{-1}$ agitates the system enough: The mobile period is significantly away from its “relaxed state”, so that the curve start higher and exhibit a steeper decay than counter-part experiments at $\dot{\gamma}^{(P)} = 0.14\text{s}^{-1}$.

The marginal case $\phi = 0.55 \sim \phi_{\text{RLP}}$ exhibits an intriguing dependence on the shear rate. One would anticipate that inter-particle force and the storage of elastic energies are small and the contacts are mostly fragile. At the shear rate $\dot{\gamma}^{(P)} = 0.14\text{s}^{-1}$, the difference between the mobile period (Δ_{On}) and the static period (Δ_{Off}) could only be even smaller than the counterparts at 0.73 and 0.64 . This fact is reflected by the much lower curve (small dots). It turns out that, only at the fast shearing $\dot{\gamma}^{(P)} = 1.10\text{s}^{-1}$, the curve shows a similarity with the high-volume-fraction counterparts, because the inertia of particles carried from the mobile period are comparable.

The dramatic change of curve as volume fraction is lowered to 0.46 simply reflects the change of physics from elastic relaxation to the flow of a suspension in which particles free float with almost no collision. The movements of all particles last longer than our observation window with the total displacements all exceeding $1d$ so that the subtraction with the reference image results in random mosaic patterns, so that the curve has a zero slope near t_{Stop} and shows a steep decay toward the noise level in the approach to the reference frame.

(Video demonstrations are available online at <http://www.phys.sinica.edu.tw/jctsai/relax/>.)

Summary and Discussion

Using hydrogel particles that are soft and slippery, we study their response to shearing in a wide range of volume fractions. At high volume fractions at which ideal hard spheres are expected to jam, the observed flow curves reveal non-trivial behaviors toward the low-speed limit (Fig.1). As we decrease the volume fraction, the shear-to-normal stress ratio reveals signs of a solid-to-fluid transition which, within our window of observation, coincides with a transition of the particle Reynolds number for a suspension (Fig.2). For a dense packing, further observations using cyclic, sudden cessations of shearing, demonstrate a multitude of relaxation timescales (Fig.3-5).

The relaxations in general reduce stress and act against the stress built-up by imposed shearing. Several questions remain open: One immediate question is what drives the relaxation of the sheared packing at the timescale of 1s and up. The consequence of the relaxation is shown not only by the non-trivial shape of flow curves (Fig.1b) where the “fast” versus “slow” regimes are set apart at the shear rate around 1s^{-1} , but also by the rearrangement of particles (Fig.5) that extends beyond 1s after the abrupt cessations of shear. Time constants constructed from simple dimensional analyses such as η/σ_N or η/E , commonly seen in theories or simulations²⁴, are in the order of 10^{-5}s or less and seem irrelevant to the time spectrum of relaxation that we describe in this work. We believe that a proper explanation must include the dynamics of sliding and, most likely, in conjunction with draining between particles or even the permeability of hydrogel that may affect the sliding. Although full answers would demand further works, there are a few clues: Our internal imaging of steady-state flows at different driving rates do reveal subtle rate dependence in the fluctuation of particles (over the mean flow). We have also note that such rate dependence become dramatic when slippery particles are replaced with frictional grains²⁵. Secondly, the evidence of the slow weakening of hydrogel itself (quite substantial at the timescale above 10^2s) with its effect on a static packing (Fig.4) also raises the question on how to interpret the steady flow curves at the “quasi-static limit” ($\dot{\gamma} \rightarrow 0$) properly, when the $1/\dot{\gamma}$ for the observation window becomes comparable to the timescale of evolution for the material. This is of vital importance as these flow curves are used for defining the yield stress, which is commonly used as the basis for studying jamming transition^{12–14}.

We hope that our survey of the shear flow and relaxation of frictionless soft particles provokes questions worthy of attention, and sheds lights on understanding the role of the softness of constituent particles on the macroscopic rheology of packed grains.

- (1) Bonn, D.; Denn, M. M.; Berthier, L.; Divoux, T.; Manneville, S. Yield Stress Materials in Soft Condensed Matter. *Rev. Mod. Phys.* **2017**, *89* (3), 035005. <https://doi.org/10.1103/RevModPhys.89.035005>.
- (2) Ikeda, A.; Berthier, L.; Sollich, P. Unified Study of Glass and Jamming Rheology in Soft Particle Systems. *Phys. Rev. Lett.* **2012**, *109* (1), 018301. <https://doi.org/10.1103/PhysRevLett.109.018301>.
- (3) Mohan, L.; Bonnecaze, R. T.; Cloitre, M. Microscopic Origin of Internal Stresses in Jammed Soft Particle Suspensions. *Phys. Rev. Lett.* **2013**, *111* (26), 268301. <https://doi.org/10.1103/PhysRevLett.111.268301>.
- (4) Negi, A. S.; Osuji, C. O. Physical Aging and Relaxation of Residual Stresses in a Colloidal Glass Following Flow Cessation. *J. Rheol.* **2010**, *54* (5), 943–958. <https://doi.org/10.1122/1.3460800>.
- (5) Bandyopadhyay, R.; Mohan, P. H.; Joshi, Y. M. Stress Relaxation in Aging Soft Colloidal Glasses. *Soft Matter* **2010**, *6* (7), 1462–1466. <https://doi.org/10.1039/B916342E>.
- (6) Mohan, L.; Cloitre, M.; Bonnecaze, R. T. Build-up and Two-Step Relaxation of Internal Stress in Jammed Suspensions. *J. Rheol.* **2014**, *59* (1), 63–84. <https://doi.org/10.1122/1.4901750>.
- (7) Ballauff, M.; Brader, J. M.; Egelhaaf, S. U.; Fuchs, M.; Horbach, J.; Koumakis, N.; Krüger, M.; Laurati, M.; Mutch, K. J.; Petekidis, G.; et al. Residual Stresses in Glasses. *Phys. Rev. Lett.* **2013**, *110* (21), 215701. <https://doi.org/10.1103/PhysRevLett.110.215701>.
- (8) Forterre, Y.; Pouliquen, O. Flows of Dense Granular Media. *Annu. Rev. Fluid Mech.* **2008**, *40* (1), 1–24. <https://doi.org/10.1146/annurev.fluid.40.111406.102142>.
- (9) Guazzelli, É.; Pouliquen, O. Rheology of Dense Granular Suspensions. *J. Fluid Mech.* **2018**, *852*, P1. <https://doi.org/10.1017/jfm.2018.548>.
- (10) Boyer, F.; Guazzelli, É.; Pouliquen, O. Unifying Suspension and Granular Rheology. *Phys. Rev. Lett.* **2011**, *107* (18), 188301. <https://doi.org/10.1103/PhysRevLett.107.188301>.
- (11) Trulsson, M.; Andreotti, B.; Claudin, P. Transition from the Viscous to Inertial Regime in Dense Suspensions. *Phys. Rev. Lett.* **2012**, *109* (11), 118305. <https://doi.org/10.1103/PhysRevLett.109.118305>.
- (12) Nordstrom, K. N.; Verneuil, E.; Arratia, P. E.; Basu, A.; Zhang, Z.; Yodh, A. G.; Gollub, J. P.; Durian, D. J. Microfluidic Rheology of Soft Colloids above and below Jamming. *Phys. Rev. Lett.* **2010**, *105* (17), 175701. <https://doi.org/10.1103/PhysRevLett.105.175701>.
- (13) Tighe, B. P.; Woldhuis, E.; Remmers, J. J. C.; van Saarloos, W.; van Hecke, M. Model for the Scaling of Stresses and Fluctuations in Flows near Jamming. *Phys. Rev. Lett.* **2010**, *105* (8), 088303. <https://doi.org/10.1103/PhysRevLett.105.088303>.
- (14) Olsson, P.; Teitel, S. Herschel-Bulkley Shearing Rheology Near the Athermal Jamming Transition. *Phys. Rev. Lett.* **2012**, *109* (10), 108001. <https://doi.org/10.1103/PhysRevLett.109.108001>.
- (15) Donev, A.; Cisse, I.; Sachs, D.; Varniano, E. A.; Stillinger, F. H.; Connelly, R.; Torquato, S.; Chaikin, P. M. Improving the Density of Jammed Disordered Packings Using Ellipsoids. *Science* **2004**, *303* (5660), 990–993. <https://doi.org/10.1126/science.1093010>.
- (16) Mukhopadhyay, S.; Peixinho, J. Packings of Deformable Spheres. *Phys. Rev. E* **2011**, *84* (1), 011302. <https://doi.org/10.1103/PhysRevE.84.011302>.
- (17) Brodu, N.; Dijkstra, J. A.; Behringer, R. P. Spanning the Scales of Granular Materials through Microscopic Force Imaging. *Nat. Commun.* **2015**, *6* (1), 1–6. <https://doi.org/10.1038/ncomms7361>.
- (18) Peyneau, P.-E.; Roux, J.-N. Frictionless Bead Packs Have Macroscopic Friction, but No Dilatancy. *Phys. Rev. E* **2008**, *78* (1), 011307. <https://doi.org/10.1103/PhysRevE.78.011307>.
- (19) Tsai, J.-C.; Tao, C.-Y.; Sun, Y.-C.; Lai, C.-Y.; Huang, K.-H.; Juan, W.-T.; Huang, J.-R. Vortex-Induced Morphology on a Two-Fluid Interface and the Transitions. *Phys. Rev. E* **2015**, *92* (3), 031002.
- (20) Keim, N. C.; Paulsen, J. D.; Zeravcic, Z.; Sastry, S.; Nagel, S. R. Memory Formation in Matter. *Rev. Mod. Phys.* **2019**, *91* (3), 035002. <https://doi.org/10.1103/RevModPhys.91.035002>.
- (21) E. Silbert, L. Jamming of Frictional Spheres and Random Loose Packing. *Soft Matter* **2010**, *6* (13), 2918–2924. <https://doi.org/10.1039/C001973A>.
- (22) Tsai, J.-C.; Voth, G. A.; Gollub, J. P. Internal Granular Dynamics, Shear-Induced Crystallization, and Compaction Steps. *Phys. Rev. Lett.* **2003**, *91* (6), 064301. <https://doi.org/10.1103/PhysRevLett.91.064301>.
- (23) Dijkstra, J. A.; Rietz, F.; Lőrincz, K. A.; van Hecke, M.; Losert, W. Invited Article: Refractive Index Matched Scanning of Dense Granular Materials. *Rev. Sci. Instrum.* **2012**, *83* (1), 011301. <https://doi.org/10.1063/1.3674173>.
- (24) Seth, J. R.; Mohan, L.; Locatelli-Champagne, C.; Cloitre, M.; Bonnecaze, R. T. A Micromechanical Model to Predict the Flow of Soft Particle Glasses. *Nat. Mater.* **2011**, *10* (11), 838–843. <https://doi.org/10.1038/nmat3119>.
- (25) <https://arxiv.org/abs/2002.07329v2>